High e+/e- Ratio Laser Pair Creation at 10^{21}W.cm^{-2}

Edison Liang[1], Taylor Clarke[1], Alexander Henderson[1], Willie Lo[1], Devin Taylor[1], Petr Chaguine[1], Ziyu Zhou[1], Yi Hua[1], Xinyi Cen[1], Wen Fu[1], Xin Wang[1], Gilliss Dyer[2], Kristina Serratto[2], Nathan Riley[2], Michael Donovan[2], Todd Ditmire[2]

[1]*Rice University, Houston, TX 77005, USA*

[2]*University of Texas at Austin, TX 78712, USA*

Abstract

Up to ~10^{11} e+e- pairs per steradian were created using ~100 Joule pulses from the Texas Petawatt Laser to irradiate gold and platinum targets, with laser intensities up to ~ 1.9x10^{21}W. cm^{-2} and pulse durations as short as ~130 fs. Positron-to-electron ratios exceeding 20% were measured on many shots, with the highest ratio reaching ~70% for a Pt rod target. This confirms that lasers with intensity ≥ 10^{21}W. cm^{-2} irradiating thick disk or rod targets are favorable for creating pair-dominated jets. We find that for thick disks and rods, Pt generally produces higher positron-to-electron ratio than gold. The maximum pair density emerging from the target is inferred to be ~ 10^{15} pairs/cm^3, making the pair plasma skin depth maginally smaller than the plasma size.

Lasers with intensities >1.4x10^{18}W.cm^{-2} couple as much as 10-50% of their energy to relativistic electrons with effective temperature kT > mc^2 [1-3]. When electrons with energy exceeding the pair-production threshold of 1.02 MeV impact high-Z target ions [4], pairs can be created via the Trident and Bethe-Heitler (BH) processes [5-10]. Cowan et al. [11,12] first

demonstrated pair creation using the Nova PW-laser, followed by Gahn et al. [13] using table-top CW lasers. However, copious pair production via the BH process was only demonstrated by Chen et al. using the Titan [14] and Omega-EP lasers [15] irradiating ~mm thick gold targets with intensities up to $\sim 10^{20}$W.cm^{-2}. These results showed that the emergent e+/e- ratio can reach a few percent and the positron yield may reach $\sim 10^{11}$ per kJ of laser energy [14-16]. For a given laser energy, a more intense laser is expected to create more energetic pairs, which can more easily escape from a thick target. Hence it is important to study the effects and benefits of higher laser intensity in ultraintense laser pair creation.

In 2012, the Texas Petawatt laser (TPW) in Austin, Texas [19] was upgraded with a new f/3 dielectric off-axis parabolic mirror donated by Los Alamos National Laboratory, which allows it to focus >100J of energy from pulses as short as 130 fs to peak intensities $>10^{21}$W.cm^{-2}. We performed 130 shots on gold and platinum targets, plus some lower-Z targets, in 2012 and 2013. During our runs, 15% of the shots achieved peak intensities $\geq 10^{21}$W.cm^{-2}. As a result the hot electrons reached very high energies. Copious gamma-rays and pairs were observed. Table 1 summarizes the laser and target parameters of our runs.

Here we first summarize the most important new results. (1) The observed e+/e- ratio exceeded 20% in many shots, with 4mm thick disk and long narrow rod targets giving the highest e+/e- ratios, reaching ~70% for one Pt rod. (2) Up to $\sim 10^{11}$ positrons/sr were detected near laser forward (LF) and target normal (TN) directions. This plus the short pulse duration allow us to infer a maximum pair density ~ 10^{15}/cm^3 emerging from the target, so that the "pair skin depth" becomes marginally smaller than the plasma size, which is the minimum requirement for creating a "pair plasma". (3) For thick disk and rod targets, Pt consistently produces higher

e+/e- ratio than Au. Hence Pt rod appears to be a strong candidate for creating pair-dominated jets to simulate astrophysical pair plasmas [22].

Three positron-electron-proton (e+e-p) spectrometers made with NdFeB magnets of 0.3T to 0.6T and 3 mm diameter pinholes were used to measure the e+e-p spectra at different angles at distances of 18 – 40 cm from the target. The spectrometers cover energy ranges of 0.5-50 MeV and 1.5-130 MeV respectively. One spectrometer was positioned near the LF direction behind the target (–11° to +3°, positive angle is measured from LF towards TN, cf. Fig.4), one near the TN direction (+25° to +40°) behind the target, and one facing the target front side at various angles. The laser was s-polarized and the laser incident angle varied between 17° and 45°. The spectrometers were calibrated using the LSU Mary Bird Perkins Cancer Center (MBPCC) clinical e-beams [26] (Fig.1a). Spectra were recorded using Fuji image plates (#BAS-IP-MS) [24,25]. The absolute dosage of the IP signal is uncertain by up to 50% due to various calibration uncertainties. Fig.1b shows typical IP images after conversion to PSL units [24,25]. The positron signal is clearly visible in both the low-energy (0.5-50MeV) and high-energy (1.5-130MeV) IPs. The proton signal from target contaminants is very bright, with peak energies between ~1 and 2 MeV. The positron signal is weak compared to the x-ray background inside the spectrometer but is concentrated in a ~4mm wide strip along the center of the magnet gap (Fig1b). Hence we developed a background subtraction procedure based on polynominal fits to the 2D background outside the central strip containing the signal. This method produced robust background-subtracted signal in which the 1-σ uncertainty is well-quantified. We tested this algorithm using Al and e-beam calibration shots in which no positron is produced, but the x-ray background level is similar. All gave null positron signal (<< 1-σ) after background subtraction. All data reported in this paper come from positron signals > 3-σ.

Fig.2a shows sample positron and electron spectra for Au targets. While the positron peak energy varies widely (5 – 25 MeV), the electron peak energy is remarkably stable (12-16 MeV) independent of target geometry, thickness and material. More significantly, the electron spectra is relatively narrow band with sharp cutoff below 3-5 MeV, which distinguishs the TPW electron spectrum from those report by other PW lasers [3,11,16]. This suggests that TPW hot electrons are acclerated by some combination of underdense mechanisms in the preplasma (e.g. LWFA-like [27]) plus critical surface mechanisms (e.g. ponderomotive [2,3]), which hints at new regimes of laser acceleration mechanisms requiring further investigation. The positron peak energies are highest for the thinnest target, consistent with sheath field acceleration [20,21]. For thick targets, the positron peak energy is lower for Pt than Au, consistent with reduced hot electrons escaping from the back surface (see below). We suspect that the differences between Pt and Au are related to the higher electrical resistivity of Pt (5 times higher than Au), which reduces the return current inside the target and partially inhibits the hot electron beam from passing through the thick target. Fig.3 summarizes the thickness dependence of the positron peak energy E_+, proton peak energy E_p and positron peak width $\Delta E(FWHM)/E_+$. There is a clear correlation between E_+ and E_p for thin targets, and clear anticorrelation between E_+ and $\Delta E/E_+$. The observed proton energy E_p is typically 10 times lower than the positron energy. If the proton energy is due to TNSA [21], this suggests that the protons, due to its slower motion, are subject to only a fraction of the total sheath field accelerating the positrons. Also both the proton and positron energy at LF is higher than at TN, contrary to conventional TNSA expectation [21]. All these results require further investigations.

Fig.4a compares the TPW e+/e- ratio vs. target thickness with the Titan data [14]. Below 3mm the two Au curves agree very well, but the TPW ratio rises steeply from 3mm to 4mm. This

shows that for laser intensities $\geq 10^{21} W.cm^{-2}$, the nonlinear rise of the e+/e- ratio with target thickness begins at 3 mm and the maximum ratio is reached only at thickness ≥4 mm,. This is because hotter electrons create higher energy bremsstrahlung photons, which in turn create higher energy pairs that can escape from thicker targets. Our data agree with GEANT4 predictions (Fig.4b) which shows the decline at 5 mm is due to the small disk diameter (4.5 mm) used in our experiment. Fig.4c shows that the ratio continues to rise at > 5 mm for much bigger disk diameters. We emphasize that the increase of the e+/e- ratio with thickness is mainly caused by increased absorption of hot electrons. The absolute positron yield actually tops out at ~ 1- 2 mm thickness. Fig.4a also shows that the Pt ratio is a factor of ~2 higher than Au at ≥ 4 mm even though it gives the same ratio up to 3mm. This is due to enhanced absorption of the hot electrons by thick Pt targets, likely related to its higher electrical resistivity.

The most interesting results come from long narrow rod targets (Fig.5a). The idea is to irradiate the end of a long narrow rod in such a way that the primary hot electrons and their bremsstrahlung photons propagate mainly along the rod axis. Since pairs are created over a broader cone than the primary electron beam, if we observe at angles away from the rod axis, then we may observe a higher e+/e- ratio by avoiding most of the primary electrons. Moreover, the long narrow rod geometry allows us to maximize the number of bremsstrahlung and pair production mean free paths, while minimizing the absorption of the created pairs emitted sideways. This conjecture is largely borne out by our TPW data (Fig.5b). The majority of the rod targets gave e+/e- ratios >15%, with one Pt rod (3mm diameter) reaching ~70%. Again Pt rods produce higher e+/e- ratios than Au rods. When the e+/e- ratio is plotted against the rod diameter*length (=DL), we find that Au rod ratios peak at DL~15mm^2. The Pt rod ratio peak

remains to be confirmed with more shots at high DL (Fig.5b). The rod data clearly suggests that one way to create a pair-dominated plasma jet is to use Pt rods.

The highest positron yields among our TPW shots are ~10^{11}e+/str. Assuming a positron emission cone of opening angle=25^{o} (~the laser incident angle for most of our shots, see also [15]), this translates into a total positron yield of ~6×10^{11} e+ per 100J of laser energy, a few times higher than those reported for Titan and Omega-EP [15], which is expected due to the higher intensity of TPW [17]. The typical positron energy of our 1- 2 mm targets is ~10 MeV, hence the conversion efficiency of laser energy into pair energy is ~10^{-2}. The typical TPW laser pulse duration is ~160 fs (Table 1). GEANT4 simulations show that the emergent TPW positron pulse duration is ~ 1 ps for an 0.35 mm thick target, translating into a plasma thickness of ~ 0.3 mm [23]. The corresponding inferred positron density is $n_{+}\sim10^{15}$ cm^{-3}. At such pair density the effective "pair skin depth" $c/(8\pi n_{+}e^{2}/m)^{1/2}$ is ~ 0.12 mm, ~ 2.5 smaller than the plasma thickness. Thus we have created a marginal "pair plasma". Future high energy lasers with intensity $\geq10^{21}$W.cm^{-2} and much longer pulse duration should easily create a true "pair plasma" with plasma size >> pair skin depth.

We believe that the emergent e+/e- ratio of our TPW experiments is systematically higher than previous experiments due to the higher laser intensity and shorter pulse. We find that long narrow Pt rods give rise to the highest detected e+/e- ratios, reaching ~70% in one case. These results provide a clear roadmap for achieving pair-dominated plasmas [22] in future laser experiments. The highest inferred pair density in our TPW experiments is ~10^{15} cm^{-3}, corresponding to a pair skin depth marginally smaller than the plasma size. This shows that future high energy lasers with intensity $\geq10^{21}$W.cm^{-2} and pulse duration much longer than TPW, should be able to create a true "pair plasma" with size >> pair skin depth. The observed TPW

hot electrons are narrow band with a well-defined stable peak at 12-16 MeV. Such hot electron spectra are similar to those currently used in elecron-beam cancer therapy [28]. Hence the application of TPW-generated hot electrons to medicine should be explored. Interestingly, the positron peak energy of mm-thick Au targets also lie in the same range (Fig.2). It is thus conceivable that such a positron beam can be used to calibrate in real-time the dose distribution received by a patient undergoing electron therapy, since the positron annihilation profile inside the human body can in principle be accurately mapped using PET technology.

This research is supported by DOE-DE-SC-0001481, the Rice University Faculty Initiative Fund, and DOE-NNSA Cooperative Agreement DE-FC52-08NA28512.

Table 1. Laser and Target Parameters

Laser Energy E_L = 81 - 130 J , $<E_L>$ ~ 100 J, < > = median value of all shots

Pulse Duration ΔT = 128 - 245 fs, $<\Delta T>$ ~ 160 fs

Peak Power P = 450 - 802 TW, <P> ~ 700 TW

Percent Energy in 10 μm circle $\%E_{10}$= 40 - 80%, $<\%E_{10}>$ ~ 65%

Peak Intensity I = $3x10^{20}$ - $1.9x10^{21}$ $W.cm^{-2}$, <I> ~ $7x10^{20}$ $W.cm^{-2}$ (15% had I ≥ 10^{21} $W.cm^{-2}$)

Laser Incident Angle = 17° - 45°; s-polarized

---

70 Gold Disks: diameter = 2mm - 6mm; thickness = 0.1mm - 5mm

30 Gold Rods: diameter = 2mm - 3mm; length = 4mm - 1cm

18 Platinum Disks: diameter = 2mm – 4.5 mm; thickness = 0.1- 6 mm

9 Platinum Rods: diameter = 2mm – 3mm; length = 4mm – 6 mm

References

1. W. L. Kruer, E.J. Valeo, and K.G. Estabrook, Phys. Rev. Lett. 35, 1076 (1975).

2. S. Wilks, W. Kruer, M. Tabak, and A.B. Langdon, Phys. Rev. Lett. 69, 1383 (1992).

3. P. Gibbon, P. *Short Pulse Laser Interactions with Matter* (Imperial College, UK, 2005).

4. J. Shearer, J. et al., Phys. Rev. A 8, 1582 (1973).

5. W. Heitler, *Quantum Theory of Radiation* (IOP, Bristol, UK, 1954).

6. E. Liang, AIP conf. Proc. No. 318, p.79, ed. G. Miley (AIP, NY, 1994).

7. E. Liang, S. Wilks, and M. Tabak, Phys. Rev. Lett. 81, 4887 (1998).

8. D. Gryaznykh, D. et al., JETP Lett. 67, 257 (1998).

9. B. Shen, B. et a., Phys. Rev. E, 65, 016405 (2001).

10. K. Nakashima, and H. Takabe, Phys. of Plasmas 9, 1505 (2002).

11. T. Cowan, et al., Laser Part. Beams 17, 773 (1999).

12. T. Cowan et al. in *High-Field Science*, p.147, Eds. Tajima, Mima, & Baldis, (Kluwer Aca./Plenum Publishers, New York 2000).

13. C. Gahn, et al. Phys. Plasmas 9, 987 (2002).

14. H. Chen, et al., Phys. Rev. Lett. 102, 105001 (2009).

15. H. Chen, et al., Phys. Rev. Lett. 105, 015003 (2010).

16. H. Chen, et al., Phys. Of Plasmas 16, 122702 (2009).

17. J. Myatt, et al., Phys. Rev. E 79, 066409 (2009).

18. A. Henderson, et al 2011, Astrophys. Sp. Sci. 336, 273 (2012).

19. M. Martinez, et all. “The Texas Petawatt Laser”. Proc. of SPIE, 5991(59911N-1), (2005).

20. R. Snavely, et al. Phys. Rev. Lett. 85, 2945 (2000).

21. S. Wilks, et al. Phys. Plasmas 8, 542 (2001).

22. E. Liang, High Energy Density Physics, 6, 219 (2010).

23. A. Henderson, et al., Phys. Plasmas, submitted, (arXiV1109.3721) (2012).

24. K. Tanaka, et al. Rev. Sci. Instr. 76, 013507 (2005).

25. H. Chen, et al., Rev. of Scientific Instruments, 79, 033301 (2008).

26. D. Taylor, et al. High Energy Density Physics 9, 363 (2013).

27. T. Tajima and J. Dawson, Phys. Rev. Lett. 43, 267 (1979).

28. K. Hogstrom and P. Almond, editors, Proceedings of the Application of Laser Particle Accelerators to Radiology Workshop (UT MD Anderson Cancer Center, Houston, 2004).

Figure Captions

Fig.1 Response functions of the high-energy (a) and low-enegy (b) magnetic spectrometers simulated using the GEANT4 code and calibrated using the MBPCC e-beams (dots). (c) Sample IP images after conversion to PSL units, showing the e+, e- and proton signals on two different spectrometers. Left IPs are from the low-E spectrometer for a 1 mm Pt target. Right IPs are from the high-E spectrometer for a 1mm Au target.

Fig.2 Positron spectra (red) compared to electron spectra (black) for sample Au targets in log-linear plots so that the high energy tail slope measures kT. All spectra are from disk targets except for the lower right figure which is from a 2 mm diameter, 8 mm long Au rod. All electron spectra peak at ~12-16 MeV while the positron peak varies by a wide range (~6-23 MeV). Positron kT is typically ~1/2 of the electron kT except for the rod target, for which the positron slope is almost as hard as the electron slope. This is likely due to the detector not seeing most of the primary electrons and also sampling pairs emitted by different parts of the rod.

Fig.3 (a) Comparison of positron spectra for different Au target thickness. Here LF refers to -8° and TN refers to +36°. Amplitudes have been renormalized to make all spectra fit on the same scale. (b) Thickness dependence of positron peak energy E_+ (circle, star), positron relative bandwidth $DE/E=\Delta E(FWHM)/E_+$ (square, diamond), and proton peak energy E_p (up, down triangles). Circle, square and up-triangle refer to data near LF (-5° to –9°). Star, diamond, and down-triangle refer data near TN (+36° to +40°). E_+ at TN is lower than at LF, whereas E_p is practically the same at the two angles. Error bars for E_+ and E_p are not shown as they are smaller than the symbol size.

Fig.4 (a) TPW emergent e+/e- ratio versus target thickness (Au: red dots, Pt: green diamonds) compared to Titan Au data (blue squares, [14]). The two Au curves track each other below 3mm,

but the TPW data rises steeply from 3mm to 4mm. At 4 mm and above, the Pt ratio is > twice the Au ratio, mainly due to the decrease of hot electrons escaping from Pt targets. Each data point represents the average of many shots and over LF and TN angles for each shot. Fig.(b) shows GEANT4 simulation results for 4.5 mm diameter disks and Fig.(c) shows results for much larger diameter disks. The GEANT4 results demonstrate that the decrease from 4 mm to 5 mm observed in Fig.(a) is due to the small diameter of the disks (4.5 mm). If we had used much larger diamter disks, the e+/e- ratio should continue to increase with thickness, though with a reducing slope (Fig.(c)).

Fig.5 (a) Sketch showing long narrow rod target experimental setup, which maximizes primary electron and gamma-ray attenuation depth along the rod axis, and minimizes attenuation depth of pairs emitted sideways. (b) Plot of e+/e- ratio for rod targets versus rod diameter*length (=DL), showing an optimal value of DL=15mm^2 for Au rods. Most of the Au rod ratios exceed the maximum Au disk ratio of 14% (dashed line, cf. Fig.4a). Pt rod ratios are also higher than Au rods, with one Pt rod reaching ~70%. Each data point represents the average of several shots and over different detector angles for each shot.

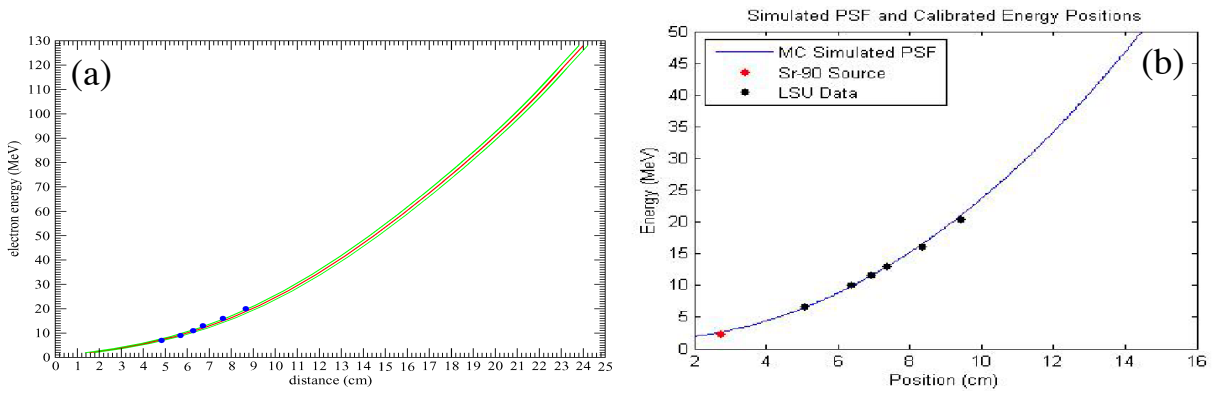

(c)

Sample e+e- Image Plate images after conversion to PSL

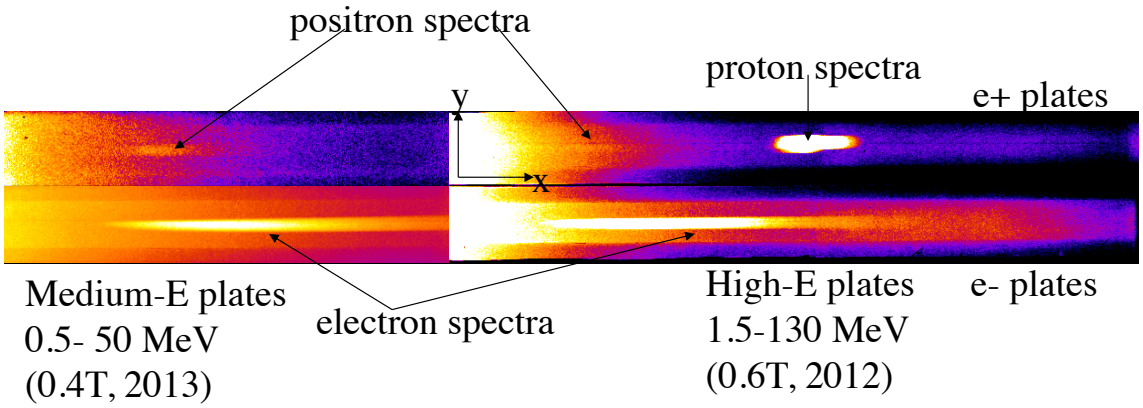

Fig.1

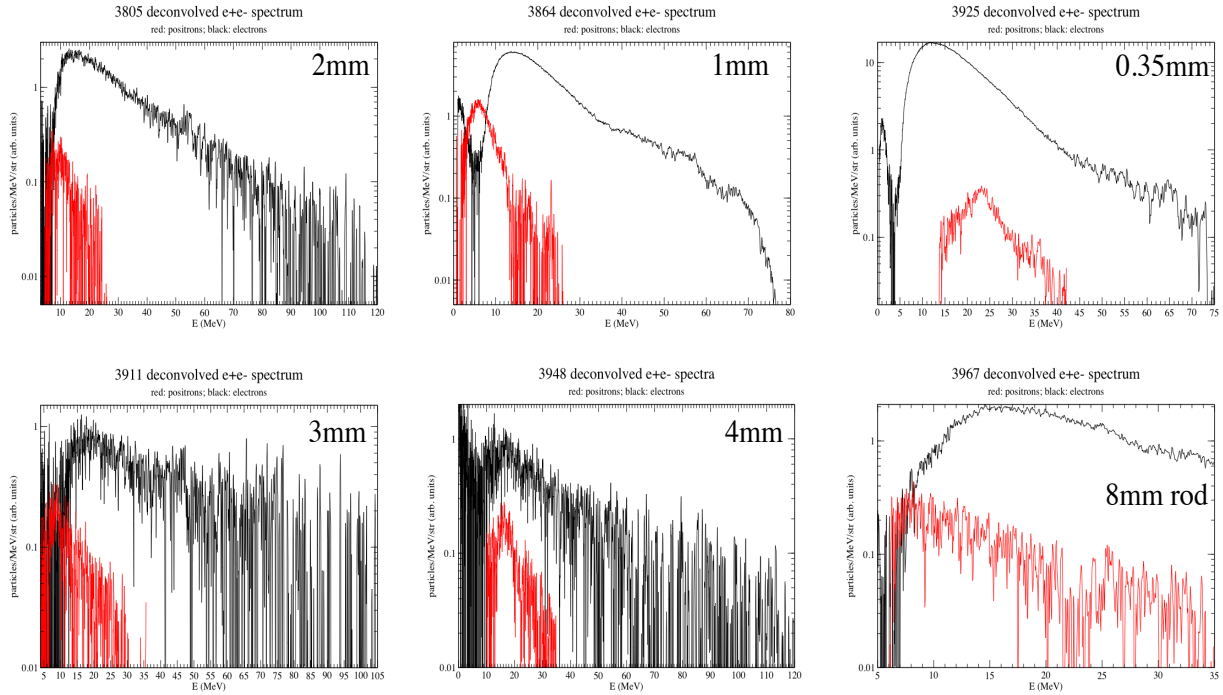
3805 deconvolved e+e- spectrum
red: positrons; black: electrons
2mm
3864 deconvolved e+e- spectrum
red: positrons; black: electrons
1mm
3925 deconvolved e+e- spectrum
red: positrons; black: electrons
0.35mm
3911 deconvolved e+e- spectrum
red: positrons; black: electrons
3mm
3948 deconvolved e+e- spectra
red: positrons; black: electrons
4mm
3967 deconvolved e+e- spectrum
red: positrons; black: electrons
8mm rod
particles/MeV/str (arb. units)
E (MeV)

Fig.2

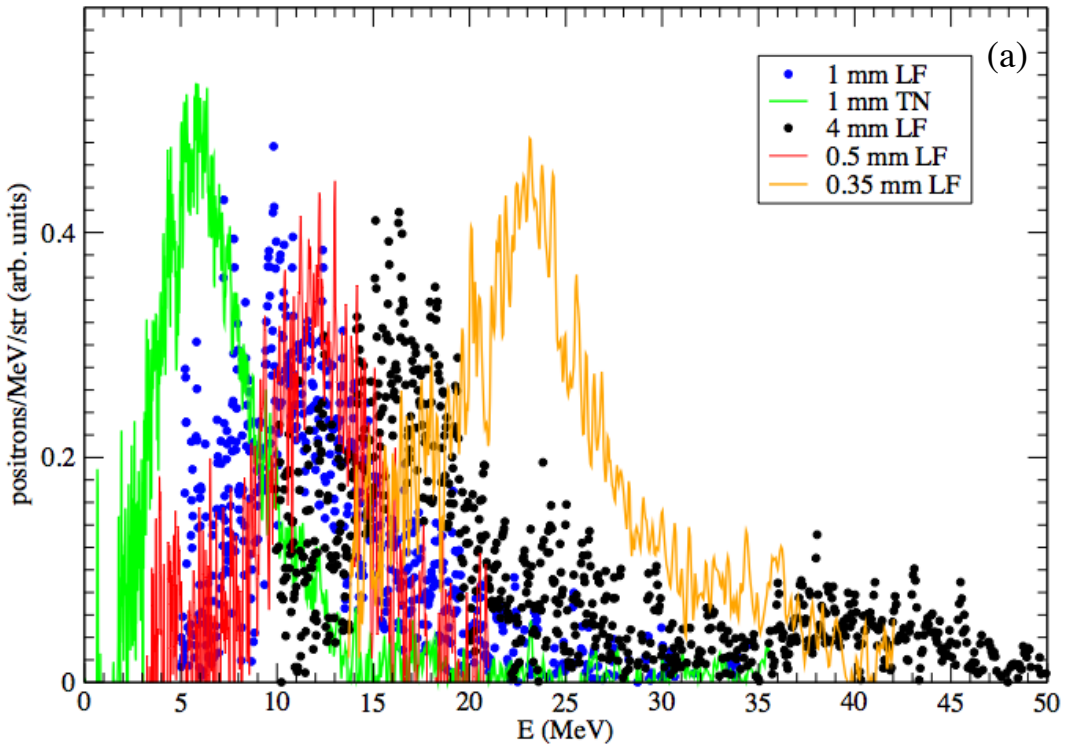
(a)
1 mm LF
1 mm TN
4 mm LF
0.5 mm LF
0.35 mm LF
positrons/MeV/str (arb. units)
0
0.2
0.4
0
5
10
15
20
25
30
35
40
45
50
E (MeV)

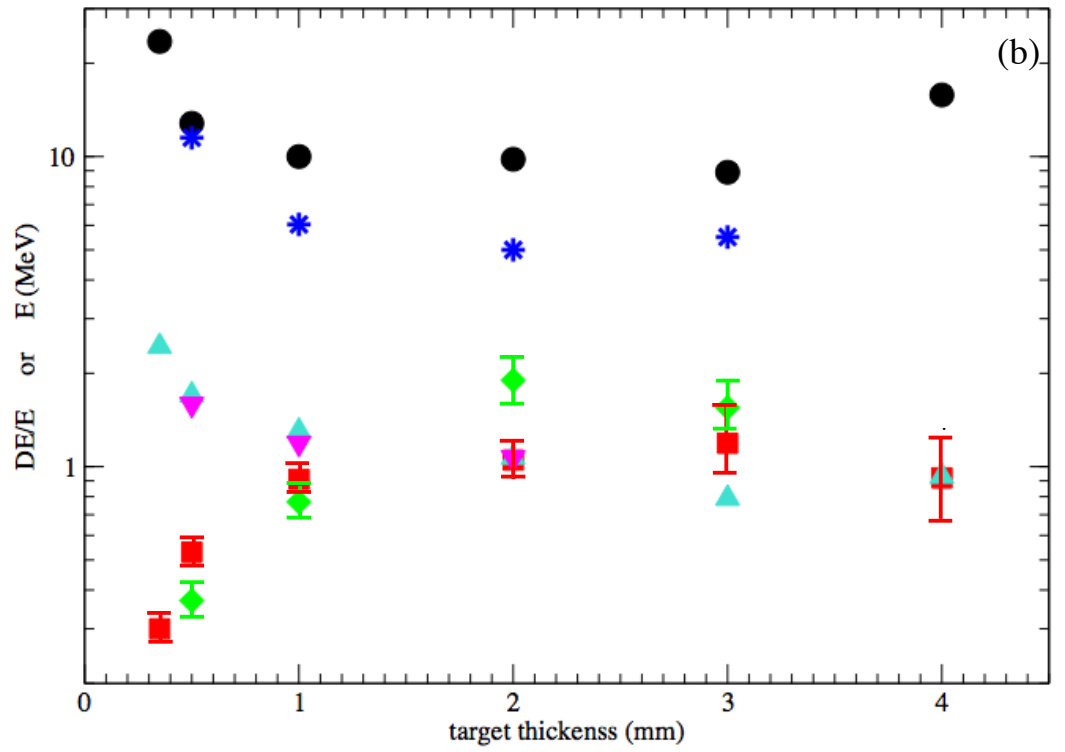
(b)
DE/E or E (MeV)
1
10
0
1
2
3
4
target thickenss (mm)

Fig.3

(a)

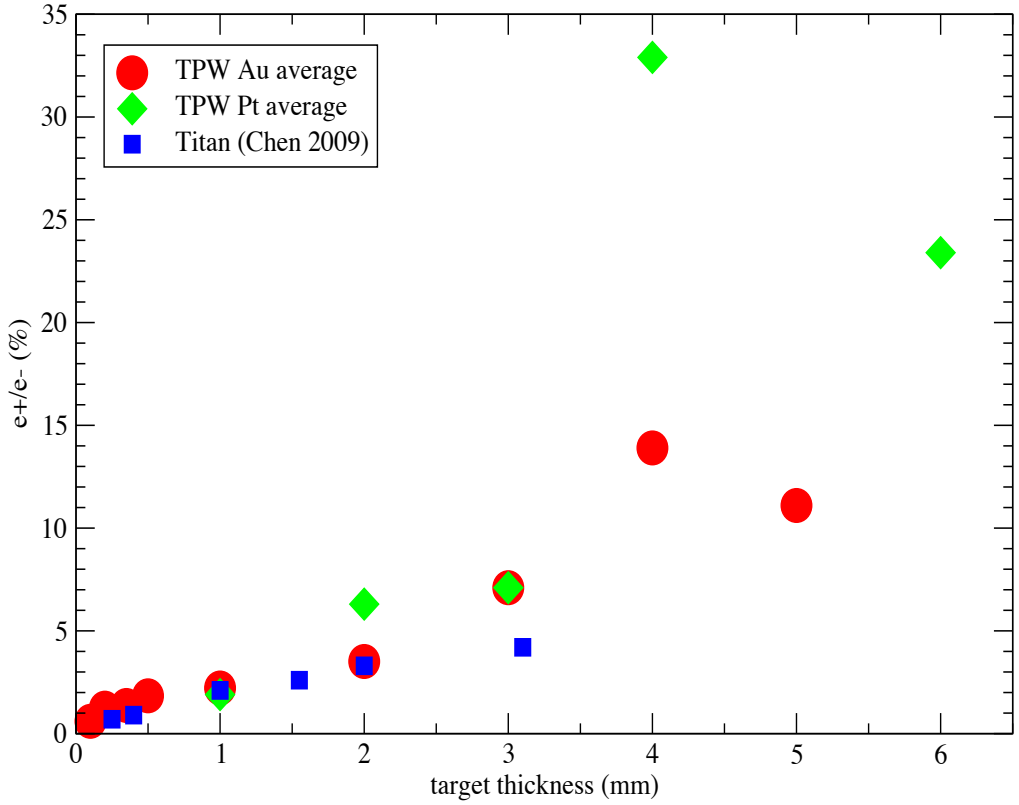
TPW Au average
TPW Pt average
Titan (Chen 2009)
e+/e- (%)
target thickness (mm)
0
5
10
15
20
25
30
35
0
1
2
3
4
5
6

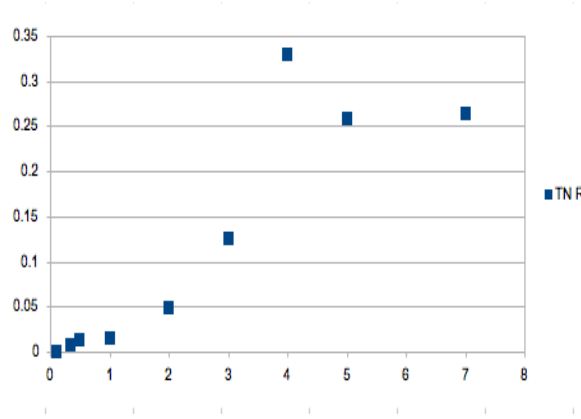
0.35
0.3
0.25
0.2
0.15
0.1
0.05
0
0
1
2
3
4
5
6
7
8
TN Ratio

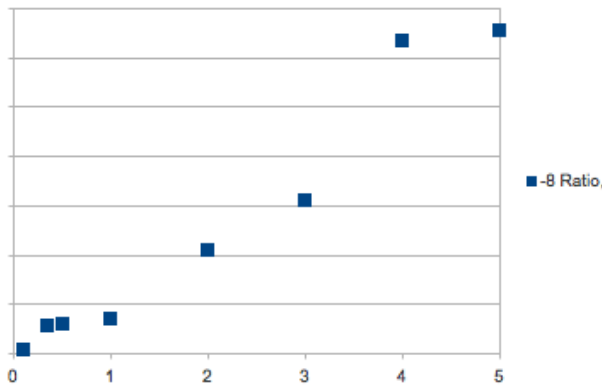
0
1
2
3
4
5
-8 Ratio

(b) (c)

Fig.4

(a)

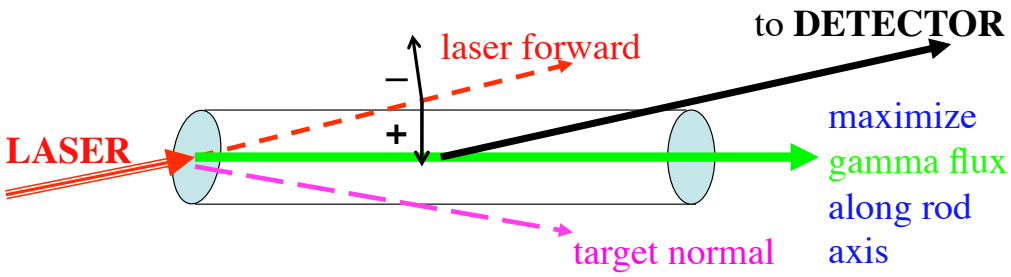

Detector needs to be positioned so as to maximize solid angle of rod visible by the detector pinhole

(b)

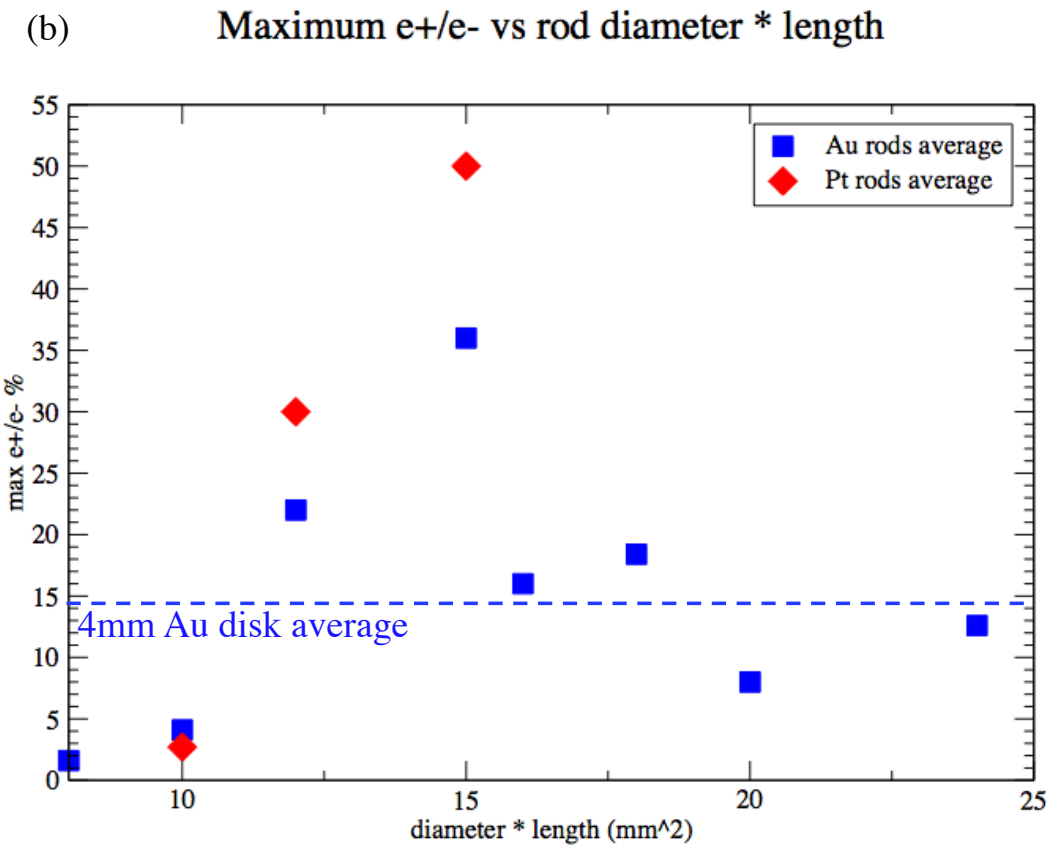

Fig.5